Role of rifting in evaporite deposition in the Great Kavir Basin, central Iran

H. RAHIMPOUR-BONAB[1], Z. SHARIATINIA[1] & M. G. SIEMANN[2]

[1]*School of Geology, College of Science, University of Tehran, PO Box 14155-6455, Tehran, Iran (e-mail: rahimpor@khayam.ut.ac.ir)*

[2]*Technical University Clausthal, Department of Mineralogy-Mineralogy-Geochemistry-Salt Deposits, Adolph-Roemer-Str. 2A-38678, Clausthal-Zellerfeld, Germany (e-mail: michael.siemann@tu-Clausthal.de)*

Abstract: The thick middle Miocene evaporites of the Great Kavir Basin, Central Iran, are classified as $MgSO_4$-poor potash-bearing deposits. In the northern domain of the Great Kavir Basin these sediments occur as 50 very large salt diapirs, as well as outcrops in several areas, including the Melheh salt pit to the south of Semnan, north Central Iran. Based on the excellent preservation of layering in these sequences, along with well-preserved bottom nucleated primary textures within the halite and sylvite, they are interpreted as largely primary deposits. They also contain some secondary minerals such as langbeinite, d'ansite, polyhalite and anhydrite. The Br content in the halite and sylvinite layers falls within the range of marine evaporites. These $MgSO_4$-poor potash-bearing evaporites deposits, along with other marine and continental sediments, appear to have been precipitated in the marginal marine basins around continental rifts. Seemingly, these evaporites formed in marginal marine rift-related basins which also received input from deep, circulating hydrothermal $CaCl_2$-rich brines. These hydrothermal brines were also rich in Fe and Zn and apparently were driven upward along faults and fracture zones by the thermal gradient along the axis of the extensional trough.

In Iran the evaporite deposits of Cenozoic age are mainly situated in the central Iran tectonic zone and its eastern sector, the northern Great Kavir Basin (Fig. 1). In the latter area these deposits, along with red beds, limestone and other marine and continental sediments, are to be found in tens of very large diapirs as well as extensive outcrops. These deposits may be divided into two stratigraphic units, and are Eocene, Oligocene and Miocene in age. They have been subject of many research projects since 1888 (e.g. Vaughan 1893; Kalhor 1961; Stocklin 1968; Neal 1969; Krinsley 1970, 1974, 1976, 1977; Russo 1976; Rowlands *et al.* 1984; Jackson *et al.* 1990; Sadedin 1990; Dari *et al.*, 1993; Rahimpour-Bonab & Alijani 2003; Rahimpour- & Kalantar-Zadeh 2007). When the Iranian Oil Company was established, one of its initial goals was to explore central Iran and the Great Kavir Basin. In the last decade preliminary potash exploration has been initiated by the Geological Survey of Iran, which has added invaluable insight concerning distribution and lateral facies changes of these deposits.

In earlier studies (Rahimpour-Bonab & Alijani 2003; Rahimpour-Bonab & Kalantar-Zadeh 2007) the origin, depositional model and diagenesis of similar Eocene and Miocene evaporites in the NW and north of the central Iran tectonic zone have been tackled. The main objectives of this study are to reconstruct the sedimentary environment of these evaporites, to examine their relationship with their equivalents in the other areas of central Iran, to decipher the possible origin of brine and potash minerals and to propose an appropriate depositional model for such thick evaporite deposits.

Geology and stratigraphy

The study area is situated in the northeastern sector of the central Iran tectonic zone, in the northern part of the Great Kavir Basin (Figs 1 & 2). The Cenozoic sediments of the central Iran tectonic zone and its eastern sector, the Great Kavir Basin, are more or less similar throughout the area, but with some regional differences. The Cenozoic of the Great Kavir Basin is an intracontinental rift basin filled with several kilometres of Eocene to Recent marine and continental sediments that are mainly evaporites, carbonates and red beds. To the south of the city of Semnan (Fig. 3) these sediments occur as about 50 very large salt diapirs that contain Eocene to Miocene evaporites, limestone and continental red beds.

This basin began to form during an important episode of rifting in the Iranian plateau during the

From: SCHREIBER, B. C., LUGLI, S. & BĄBEL, M. (eds) *Evaporites Through Space and Time.* Geological Society, London, Special Publications, **285**, 69–85.
DOI: 10.1144/SP285.5 0305-8719/07/$15.00

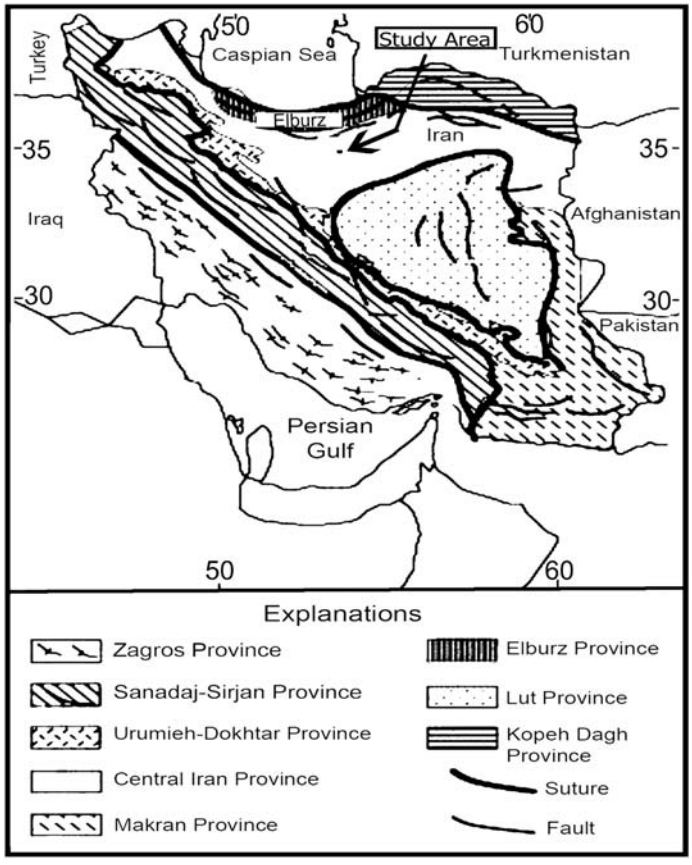

Fig. 1. Tectono-sedimentary provinces of Iran and location of the studied area (map from Geological Survey of Iran; National Iranian Oil Company 1977).

Early Cretaceous and this area became a region of intense and pervasive block faulting during rifting. Evidence for this style of tectonism is present as horst and graben structures that underlay the Kavir Basin. In these rift grabens, best developed in the northeastern border region of the Kavir, the sequence comprises sediments that range from Upper Cretaceous to Recent (Stocklin 1968).

Most authors favour the idea of a wide (Neo-) Tethys ocean passing through Iran from Mesozoic until the Eocene (Belov *et al.* 1986; Dercourt *et al.* 1986; Scotese 1987). Accordingly, the ophiolitic mélange zones exposed in the north of the Great Kavir fault are remnants of an old ocean floor that had completely encircled and isolated a Central Iran microcontinent (Fig. 3). Consequently, distribution of the mélange zones and their lateral discontinuity in the Great Kavir Basin suggest a pattern of strongly subsident rift grabens and narrow troughs of ocean crust separated by relatively stable horsts (Jackson *et al.* 1990). Since that time, at least up to the Eocene, this oceanic crust was largely subducted leaving remnants of oceanic crust and its associated sediments in different parts of Central Iran, including the Great Kavir Basin and the Zagros suture zone. Although evaporites of the Great Kavir Basin first appeared in small, scattered sub-basins in the Early Middle Eocene, significant evaporite deposition began during regional regression toward the end of the Eocene. This regression was related to an important phase of faulting, tilting and regional uplifting that affected all of central Iran. These changes in the relative plate movements, during Eocene times (Dewey *et al.* 1989), were associated with subduction-related volcanism that affected central Iran. Owing to these tectonic events, the setting changed from the marine sediments of Lower to Middle Eocene and passed up into thick continental red bed facies of the Lower Red Formation (LRF) during the Oligocene (Fig. 4). The LRF, which is composed of red continental clastics and evaporites

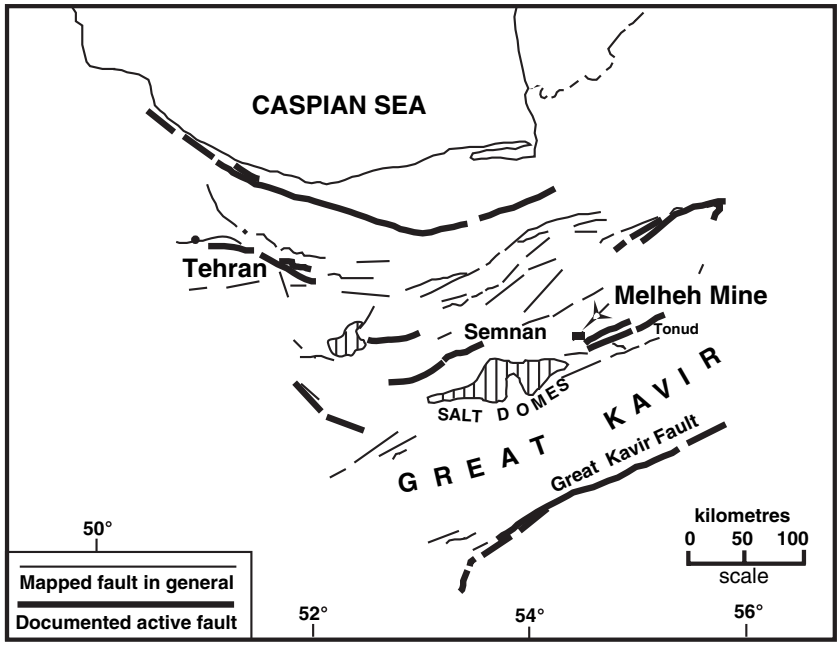

Fig. 2. Main fault system and distribution of diapirs in the Great Kavir Basin (Jackson *et al.* 1990, with permission from GSA).

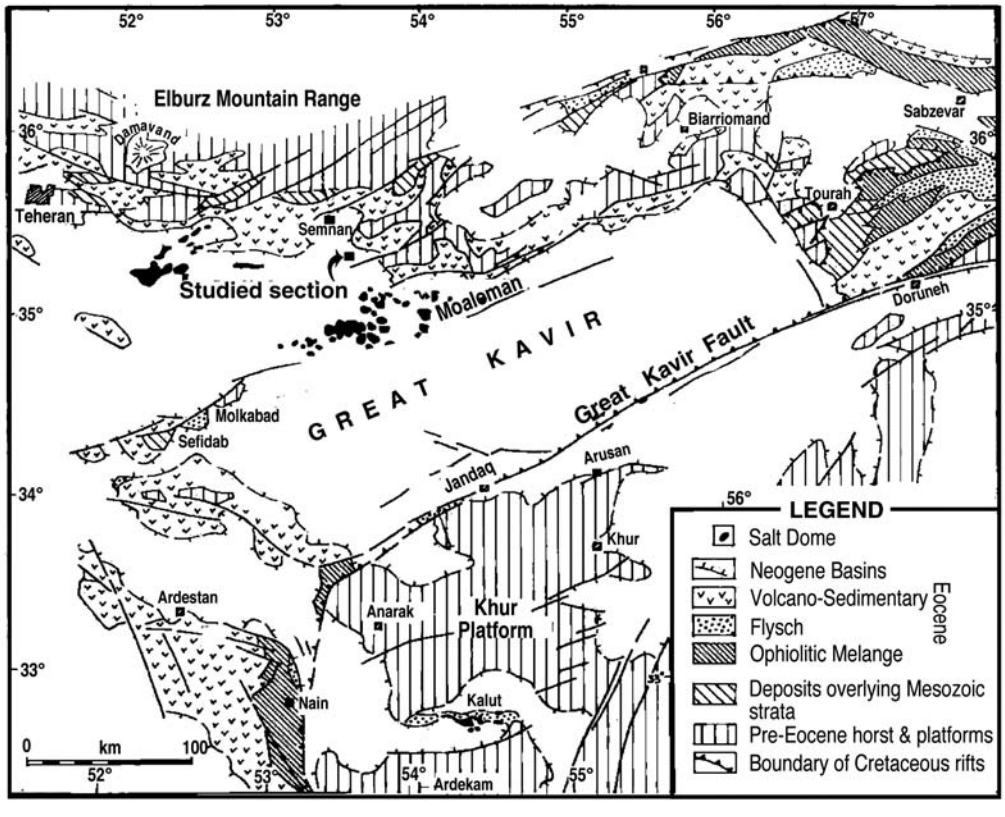

Fig. 3. Diapirs, salt flat and ophiolitic mélange distribution in the study area (Jackson *et al.* 1990, with permission from GSA).

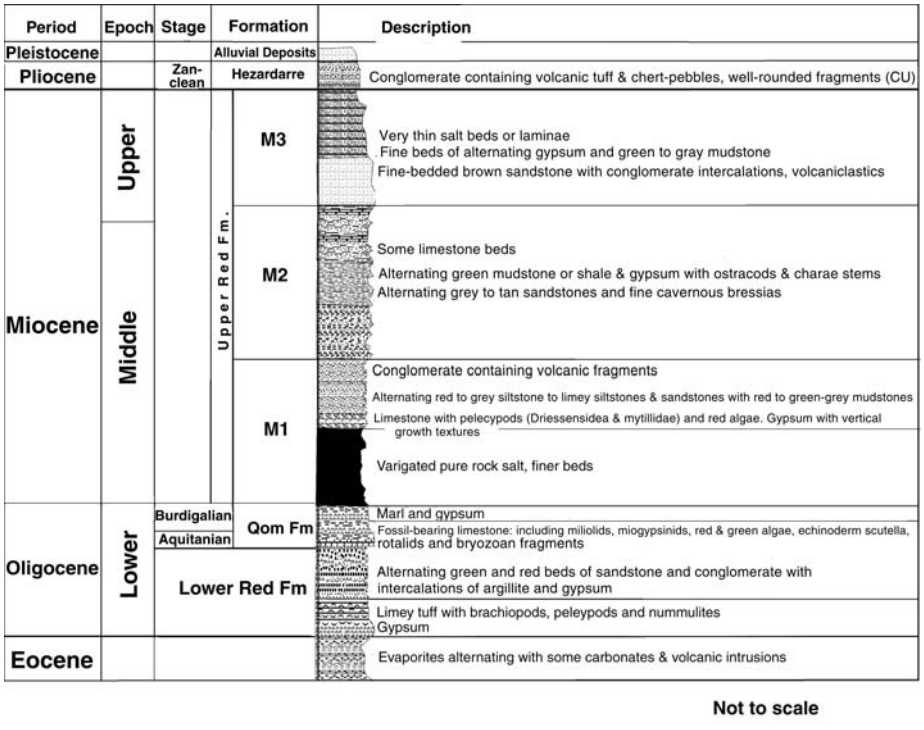

Fig. 4. Stratigraphic column of the studied area in the Northern Kavir Basin.

of Oligocene age, marks the onset of a new sedimentary cycle. The evaporite units of the LRF, which crop out in the northern border of the central Iran tectonic zone, in the Great Kavir Basin (south of the city of Semnan) and are present in its very large diapirs, are marine in origin (Rahimpour–Bonab & Alijani, 2003). These evaporites are mainly halite with some potash layers that have simple mineralogy, with high bromine content (up to 450 ppm) and are associated with some marine limestone.

The retreat of the sea in the Early Miocene (Burdigalian) led to the establishment of continental wadi conditions, and the marine limestone of the Qom Formation was gradually replaced by thick evaporite and continental red bed facies of the Upper Red Formation (URF). The lithologies of the Upper Red Formation are very similar to the LRF. Thus, in the Middle Miocene development of restricted marine conditions produced a facies change from the shelf carbonates of the Qom Formation to evaporite sequences of the M1 member, Upper Red Formation (URF) (Rahimpour-Bonab & Kalantar-Zadeh in press). This basal evaporite member (M1), is about 200 m thick and is mainly composed of gypsum, halite and in some places potash minerals, in the type section, overlying the uppermost marine marl of the Qom Formation.

The area of the Melheh salt pit is located in the M1 unit and there its thickness is more than 800 m (Figs 5 & 6). Seemingly, this evaporite member is a lateral equivalent of massive reef limestone, which in some areas of the Central Iran is classed as the uppermost member of the Qom Formation. The M1 member demonstrates a partial lateral transition from the Qom limestone to evaporites. Above this basal evaporite are about 2000 m of red-bed continental sediments with distinct repetitive series composed of shale, siltstone, mudstone and sandstone. Each series is from 10 to a few tens of metres thick and comprises from bottom to top: impure salt, gypsum, green gypsiferous mudstone and red claystone. Apparently, the sequences represent a reversal of a typical (marine) evaporite sequence by a periodic influx of relatively fresh water into the highly concentrated brine of a landlocked basin dominated by arid climate.

Member M2 is 2000–3000 m thick and is composed of an alternation of gypsiferous mudstone and siltstone with distinct colour banding. In the middle part of this member numerous intercalations of pale green marl (up to 500 m in thickness) that contain abundant ostracodes and Chara oogonia are also

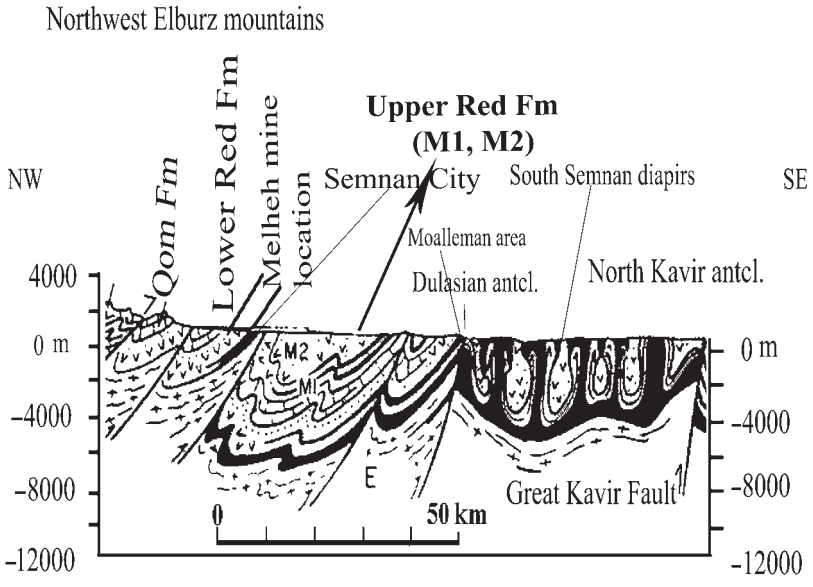

Fig. 5. Schematic cross section across the Great Kavir Basin. Salt units are in black (modified from Jackson *et al.* 1990, with permission from GSA).

present. This part is overlain by fine-grained grey sandstone that contains some conglomeratic (pebble) intercalations.

Member M3, having about 1000 m thickness, consists of sandstone with intercalations of conglomerates overlain by cyclic saline mudstone with grey to green colour.

Overall, the URF sequences are made up of a facies mosaic of lagoonal and salina evaporites (mainly halite beds) admixed with continental siliciclastics that conformably, and in some places gradually, overlies the Qom Formation (Rahimpour-Bonab and Kalantar-Zadeh 2007). Most of the extensive red beds exposed in the Kavir Basin and central Iran belong to the URF. In the northern border of the Kavir, the URF is well exposed in the large Moalleman anticline, southeast of the Melheh salt pit (Fig. 5). This unit overlies the palaeontologically dated topmost Burdigalian beds of the Qom Formation and lies below an unconformable overburden of continental deposits, which in NW Iran contain a freshwater fauna of Zanclean (Early Pliocene) age. Thus the URF in central Iran and Kavir Basin is between 17 and 5 Ma old (Jackson *et al.* 1990).

The structural trends of the area follow the major structural elements of the region, i.e. the Alborz Main Fault and Zagros Trust Fault (Jackson *et al*. 1990; Fig. 7). By mid Miocene time significant orogenic movements ceased in the Middle East (Late Alpine orogeny). This resulted in the development of several shallow basins that then were filled by evaporite and continental sediments (Jackson *et al.* 1990; Darvishzadeh 1991). In the northern province of the central Iran tectonic zone and in the Zagros Basin shallow discontinuous

Fig. 6. Outcrop photo showing well-preserved layering in the halite of the Melheh salt pit.

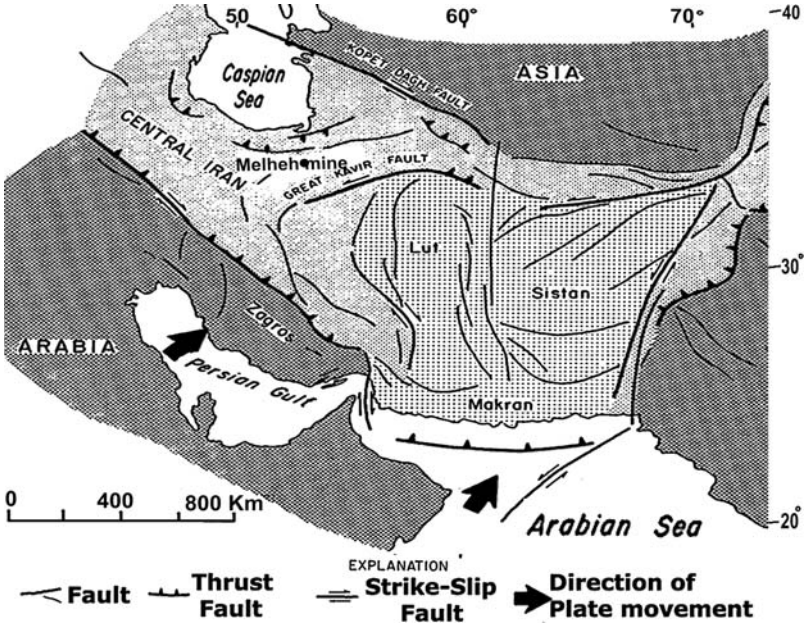

Fig. 7. Map of plate tectonic setting of central Iran and adjacent micro-plates between converging Arabian, Indian and Asian plates. Complied from Gansser (1974); Stocklin (1984); and Dercourt *et al.* (1986) (with permission from GSA).

epicontinental settings were dominated by an arid climate, and became the sites of widespread evaporite deposition and continental wadi sediments. This phase of evaporite deposition was interrupted several times and such deposits are diachronous all over central Iran.

Methods

This paper is based on the field study and petrographic examinations (thin sections and XRD) and geochemical analysis (Br, K, Ca, Mg, Zn, Fe) of the core material and salt pit samples. Accordingly, about 200 samples were systematically collected at regular intervals (1 m) from outcrops and boreholes of the Melheh salt pit in order to decipher the depositional environment and diagenesis of evaporite deposits. Samples that showed minimal post-depositional alteration, with well-preserved syndepositional textures, have been used for geochemical analysis.

The chemical composition of minerals was analysed by ion chromatography. Major anions and cations in the solutions were measured simultaneously after dilution by a factor of 5000–10,000 by use of a Metrohm ion chromatograph with chemical suppression for the anions. All samples were acidified to a pH of 2.6. Accuracy and reproducibility were investigated by analysing the North Atlantic Standard Seawater (NASS4) international reference sample ($n - 50$). The accuracy was better than 1% (relative) for all elements except for K (<4% relative). The relative standard deviation for the analysis of the reference sample was 1% except for K (<3%) (Siemann & Schramm 2000).

Br in the crystals was analysed in neutral solution after they were diluted 1:1000. Accuracy as well as reproducibility was better than 1% measured against an in-house halite reference sample. The calibration for the Br quantification was strongly adapted to the Cl concentration of the crystal. Before dissolving the crystals, they were analysed by laser Raman spectroscopy (Siemann and Ellendorff 2001) and X-ray powder diffraction (Siemann 1993).

Petrography and diagenesis

In this study area the sedimentary sequence, from base to the top, is composed of following units.

Evaporite sequences

These can be subdivided into three units.

A chloride unit This unit, which is very well-bedded (Fig. 6), having more than 800 m thickness, is strongly variegated and shows alternations of various colours in different scales (Fig. 8). In the

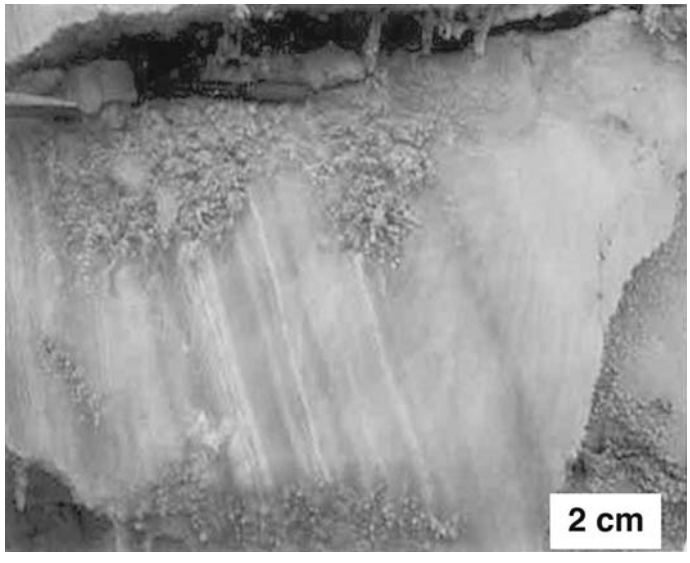

Fig. 8. Well-preserved lamination with variegation in halite sample from Melheh salt pit.

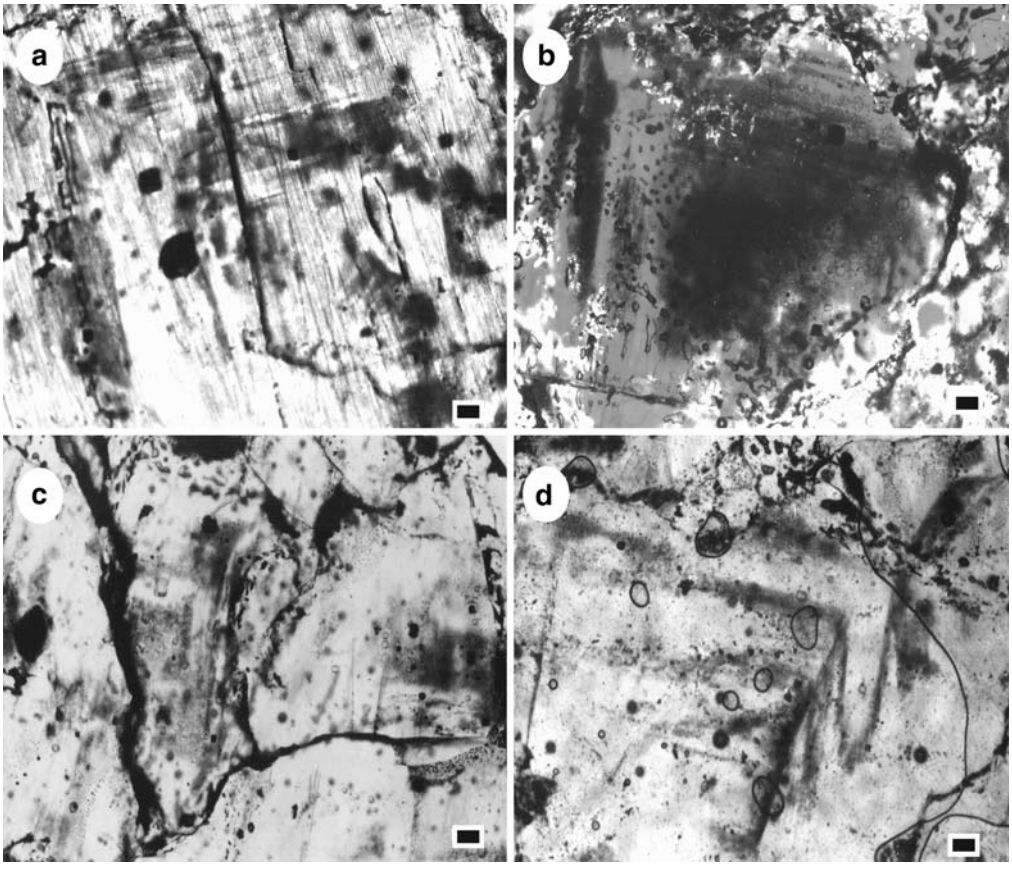

Fig. 9. Salt growth structures (scale bar for all figures 250 μm). (**a**) Vertically elongated chevron textures (plane polarized light). (**b**) Halite cornets (polarized light and gypsum filter) in halite. (**c**) Vertically elongated halitechevron textures and cornets (plane polarized light). (**d**) Halite in sylvite (plane polarized light).

Melheh mine, the blue to violet colours in halite are of great interest, because they are used as key beds for prospecting for potash-bearing layers (sylvinite beds). They are restricted to the contact zone between halite and sylvinite. Discoloration is attributed to water percolation along bedding planes that induces recrystallization (Sonnenfeld 1995). Accordingly, bromine is leached by circulating brine (from NaBr), but metallic Na remains intact and that produces blue colours (Sonnenfeld 1995).

The chloride unit is composed of the following paragenetic assemblage: primary minerals that include halite, gypsum, sylvite (KCl) and carnallite ($MgCl_2 \cdot KCl_2 \cdot H_2O$). However, based on the petrographic examinations, the secondary minerals are polyhalite ($2K_2SO_4 \cdot CaSO_4 \cdot MgSO_4 \cdot 2H_2O$), langbeinite ($2MgSO_4 \cdot K_2SO_4$), d'ansite ($9Na_2SO_4 \cdot MgSO_4 \cdot 3NaCl$), anhydrite ($CaSO_4$), plus minor amounts of dolomite and ankerite. In addition, some tiny particles of reworked volcaniclastic minerals are present in the studied thin sections.

Based on the chemical groupings proposed by Hardie (1984) the studied evaporites can be classified as $MgSO_4$-poor potash-bearing deposits, made up of cycles composed of halite, sylvite and subordinate carnallite, which show delicately, well-preserved, primary depositional bottom-growth textures. In thin sections of halite and sylvinite beds, many halite and sylvite crystals show remarkable preservation of depositional textures, fabrics and primary fluid inclusion banding. Both minerals commonly exhibit vertically elongated chevron textures with cloudy fluid inclusion bands outlining primary crystal growth faces (Fig. 9). Some halite and sylvite layers show well sorted millimetre-sized or larger cumulate crystals (Fig. 10) and centimetre-sized, randomly oriented hoppers, with fluid inclusion banding, now filled with clear halite cement (Fig. 10). These primary textures are evidence of growth in a shallow brine pool (e.g. Philips 1956; Llewellyn 1968).

Thus, sylvinite layers are largely interpreted as primary deposits, because the sylvite is intergrown with halite and both contain unquestionable primary subaqueous textures (Fig. 10) and they show no evidence of an origin by replacement. In many cases they do show polygonal-mosaic textures, with individual halite and sylvite crystals with various sizes. The other common texture observed in sylvinite beds is a framework of euhedral and subhedral halite cubes, poikilitically enclosed by anhedral crystals of sylvite. Carnallite

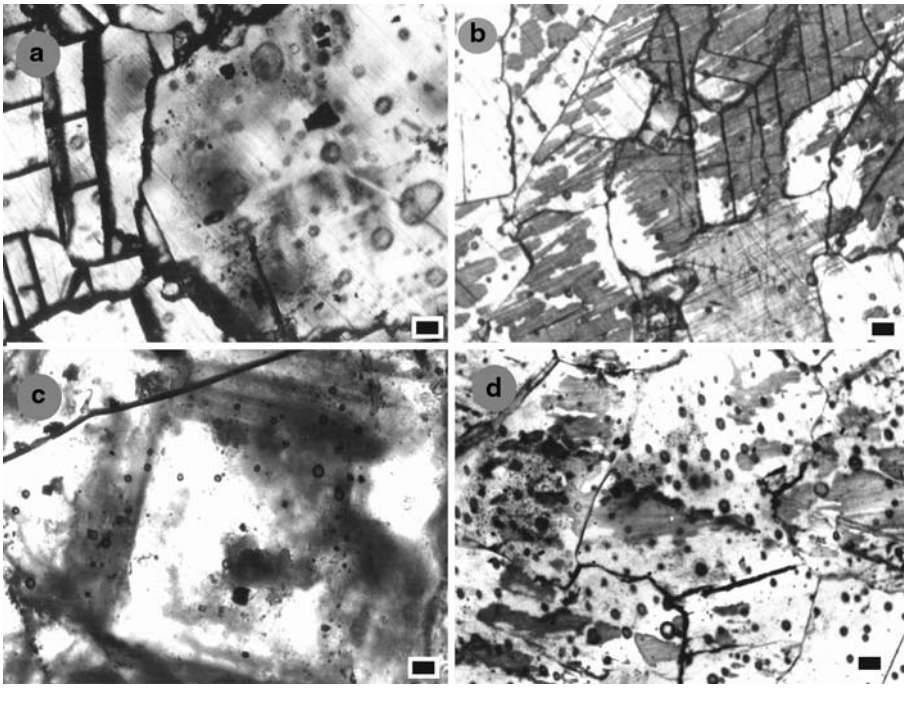

Fig. 10. Salt growth structures (all figures in plane polarized light, scale bar 250 μm). (**a**) Well-sorted millimetre-sized cumulates crystals of halite. (**b**) Well-sorted millimetre-sized cumulates crystals of sylvite. (**c**) Centimetre-sized, halite hoppers with fluid inclusion banding, which are filled with clear halite cement. (**d**) Intergrowth of primary sylvite and halites crystals.

occurs as tiny anhedral crystals between framework crystals of halite and sylvite within the sylvinite layers. Textural evidence suggests a syndepositional cement origin for such carnallite.

Absence of alteration rims around sylvite crystals rules out the possibility of their secondary origin. Surface nucleated halite crystals (such as pyramidal hoppers) are present and commonly associated with primary crystals of sylvite (Fig. 11). This texture not only indicates primary deposition but also denotes either settling in a stratified brine body or very rapid evaporation in an unstratified system (Hardie *et al.* 1985). Periodic refreshment and renewed stratification may have inhibited saturation of the brine column (Kovalevich 1978). As a result, in the stratified brine pool, co-precipitation of sylvite occurs as bottom nucleated crystals. In addition, the sylvinite layers follow the depositional boundaries of well-preserved halite layers.

In the K-salt-bearing horizons, potash is present both as primary and also secondary minerals that comprise up to one-third of the sequence. Secondary potash minerals such as polyhalite, d'ansite and langbeinite are confined to the crystals boundaries of primary halite crystals (Fig. 11).

Some sylvite crystals form millimetre-sized anhedral mosaics which lack fluid inclusion banding (Fig. 11), but in most instances sylvite is composed of millimetre-sized chevrons. Mosaic textures of sylvite crystals were probably produced by post-depositional modification (diagenetic neomorphism) of sylvite crystal boundaries. One possible modification mechanism for primary textures of the sylvite crystals, during early diagenesis, is via a 'brine curtain' mechanism (Warren 1999, pp. 80–81). Lack of the extensive cementation by primary potash minerals in the halite layers indicates that the primary potash minerals were formed rapidly, before the brine could reach the desiccation stage.

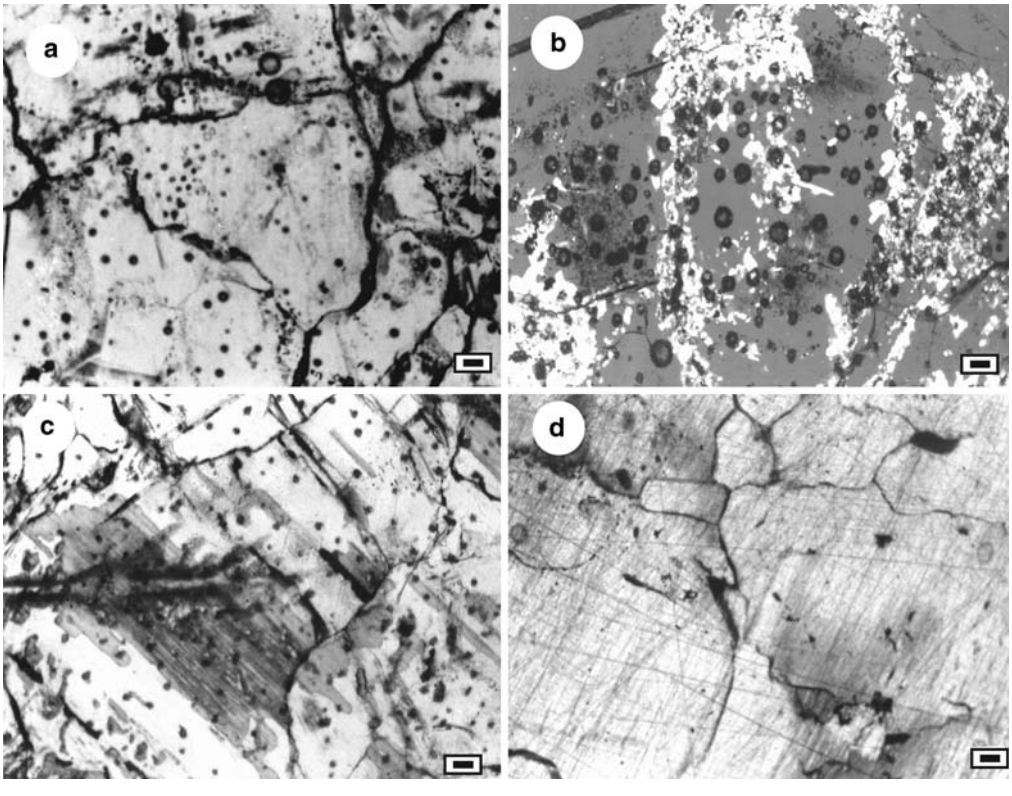

Fig. 11. Photomicrographs of various salts (scale bar for all figures 250 μm). (**a**) Hopper halite crystals associated with primary crystals of sylvite (plane polarized light). (**b**) Secondary potash minerals (such as polyhalite, d'ansite and langbeinite) are confined to the crystals boundaries of primary halite crystals (polarized light and gypsum filter). (**c**) Sylvite crystals form anhedral mosaics which lack fluid inclusion bandings associated with primary sylvite with chevron texture (plane polarized light). (**d**) Halite with drusy mosaic texture showing curved crystal boundaries meeting at triple junctions, (plane polarized light).

Moreover the absence of mud partings supports the latter conclusion.

In some cases halite chevrons are truncated by irregular patches of clear halite that enclose the cloudy traces of the primary textures. Seemingly, this feature is an indication of syndepositional dissolution–precipitation periods and represents partial recycling of the concentrated pore fluids in the micropores of newly precipitated halite crystals (Kirkland *et al.* 2000). Thus, the clear halite crystals are early diagenetic cements (Shearman 1978; Spencer 1987).

In a few samples halite crystals lack any syndepositional features and rather display diagenetic textures such as inclusion-free equigranular mosaic crystals with curved boundaries that meet at triple junctions (Fig. 11). These observations along with the preservation of the primary textures in most samples suggest an early stage of shallow burial diagenesis.

In the chloride unit anhydrite and gypsum and secondary potash minerals, such as polyhalite, d'ansite and langbeinite), occur as alteration haloes confined to the boundaries of the halite and sylvite crystals (Fig. 11). In this unit anhydrite and gypsum are also present as nodules and microcrystalline aggregates. Presumably, secondary potash minerals, such as polyhalite, formed by partial alteration of sulphate nodules. This may suggest that the secondary potash minerals have been formed due to chemical reactions between sulphate nodules and Mg and Ca-rich fluids. Presumably these concentrated pore fluids were released from primary inclusions in the capillary fringe (Hardie *et al.* 1985; Peryt *et al.* 1998). This type of anhydrite and gypsum transformation to polyhalite is an indication of interactions between sulphate-bearing diagenetic fluids with the K-bearing host mineral such as sylvite. Association of diagenetic ankerite and dolomite crystals with polyhalite is another indication of high Ca and Mg content of these diagenetic fluids.

Sulphate beds Toward the uppermost section of the chloride unit the pure halite and sylvinite beds gradually change to the alternations of halite and gypsum that signal the end of halite deposition. In this part of the section about 50 m of gypsum, composed of vertically aligned primary vertical crystals (fibrous), overlies the chloride unit with sharp contact. These sulphate beds are overlain by a marine, fossil-bearing, carbonate unit having approximately 30 m thickness.

Carbonate unit This unit sharply overlies the latter beds and contains copious marine fossils including molluscs such as mytillidea, cardidea and dreisinsidea, microfossils such as some species of milliolidea, and other marine biota such as red algae, green algae and corals. The lower parts of the carbonate unit, which is thick bedded limestone, contains plentiful quantities of marine micro- and macrofossils of shallow-water organisms. However, toward the top, due to facies change, the abundance and diversity of fauna and flora diminishes and thick-bedded marine limestone passes upward into red, sandy, fine-bedded limestone. This suggests that, after deposition of the sulphate beds, open marine conditions returned to the area; however, a gradual facies change from marine fossiliferous limestone to marginal, sandy, non-fossiliferous carbonate signals the onset of another marine regression.

Siliciclastic sequences

The carbonate unit is overlain by very thick sequences (up to 1.5 km) of siliciclastic continental sediments (red beds) that contain red to grey sandstone, mudstone, siltstone, marl and conglomerates, mainly composed of volcaniclastic fragments. These belong to the upper parts of M1 and M2 members. Presumably, they demonstrate permanent marine retreat from the Great Kavir Basin, and considerable subsidence to create the capacity for the accumulation.

Geochemistry

Evidently, potash deposits that contain primary sylvite and carnallite and lack $MgSO_4$ salts have been precipitated from Na–Ca–Mg–K–Cl brines (Hardie 1984). Normally, upon evaporation seawater may reach 70–100 times its original concentration. Usually, at this stage the brine is depleted in SO_4, and Ca (due to formation of either gypsum or anhydrite), and will be relatively enriched in Mg, K and Br. The high Br content of such concentrated brines is due to the high concentration of 0.84 mol Kg^{-1} H_2O in seawater (Braitsch 1971; Bruland 1983) and its long residence time (1.0×10^3 years) in the ocean (Chester 2000). Accordingly, the Br content of the halite could provide invaluable insight about depositional conditions and brine evolution of halite- and sylvite-bearing evaporites. Additionally the Br partition coefficient between halite and brine is about 0.12–0.14 (Schreiber & El Tabakh 2000; Siemann & Schramm 2000, 2002). Thus, at the beginning of the potash precipitation stage the highly concentrated brines are significantly enriched in Br. This partition coefficient is affected by other ionic species in the brine, such as K^+, HCO_3^- and Ca^{+2} (e.g. Braitsch & Herrmann 1963; Siemann & Schramm 2002). Accordingly, the Br content of

Table 1. *Bromine concentration in the halite and sylvite samples from Melheh salt pit*

Sample no.	Br(ppm)	Sample no.	Br(ppm)
1-1	140	26	203
1-2	105	27	256
2	100	28	79
3	112	29	170
4	136	30	195
5	137	31	114
6	124	32	225
7-1	159	34	216
7-2	99	35	202
8	157	36	85
11	197	37	207
12	179	38	184
13	175	39	196
13-1	155	40	215
13-2	162	41	203
14	143	42	305
15	186	43	211
16	232	44	219
17-1	162	45	224
17-2	204	46	49
18	194	47	241
19	181	48	207
20	167	49	196
21	197	54	226
22	190	64	168
23	220	70	169
24	205	72	172
25	199	75	155

the halite deposits could provide invaluable insight about depositional conditions and brine evolution of halite- and sylvite-bearing evaporites. Finally there is one other factor in this consideration, the dissolution of older salts into the brine, as in the case of the Dead Sea (Zak 1997).

The Br content in the primary halite layers, those that show well-preserved depositional textures, is about 60–140 ppm but rises to 200–300 ppm in sylvinite beds (Table 1). The Br content of the secondary diagenetic samples (clear halite), those halites which show triple junction boundaries, is about 49–75 ppm. This secondary texture could have been formed by dissolution during diagenesis (Holser 1979) or by partial recycling of diagenetic fluids released during the gypsum–anhydrite reactions (Kirkland *et al.* 2000). Mean Br values of the sylvinite layers are about 330 ppm, implying that the brine was already sufficiently concentrated to crystallize carnallite. These values demonstrate that the parent brine had evolved to the potash level deposition.

Based on Br values, the bromine profile of the chloride unit may be divided into three parts. Halite samples with less than 60 ppm Br were influenced by late diagenesis while halite crystals with primary textures show Br values of about 65–190 ppm. Higher Br values (up to 305 ppm) belong to sylvinite layers (Fig. 12). Vertical Mg and K profiles approximately correlate with the latter values, which suggests a primary signature for Br (Fig. 13). In most samples Ca values correlate negatively with the other elements, except where secondary Ca-sulphate minerals are present. In halite samples Zn values vary between 200 and 1250 ppm and Fe from 100 to 943 ppm (Table 2). These values, which are higher than the average for marine evaporites, suggest a contribution of hydrothermal brines (Hardie 1990).

Fluid inclusions

Petrographic examination of halite and sylvite reveal well-preserved fluid inclusions along growth bands of halite and sylvite crystals, with their typical rectangular shape (Fig. 10). There are also some secondary anhedral inclusions that show irregular shape and formed during diagenesis. Based on Bodnar's (1994) classification, there are three types of inclusions recognized in the studied samples that include primary monophase fluid inclusions, primary polyphase inclusions and secondary polyphase inclusions, which are located at the grain boundaries. The primary inclusions range in size from 10 to 100 μm, but the secondary inclusions are much larger.

Some sylvite crystals, with well-preserved fluid inclusion bandings (such as chevrons), contain

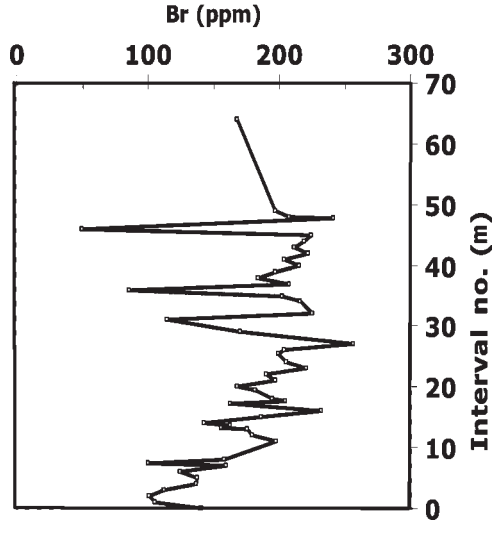

Fig. 12. Vertical bromine profile of the Melheh salt pit (depth from top of the section).

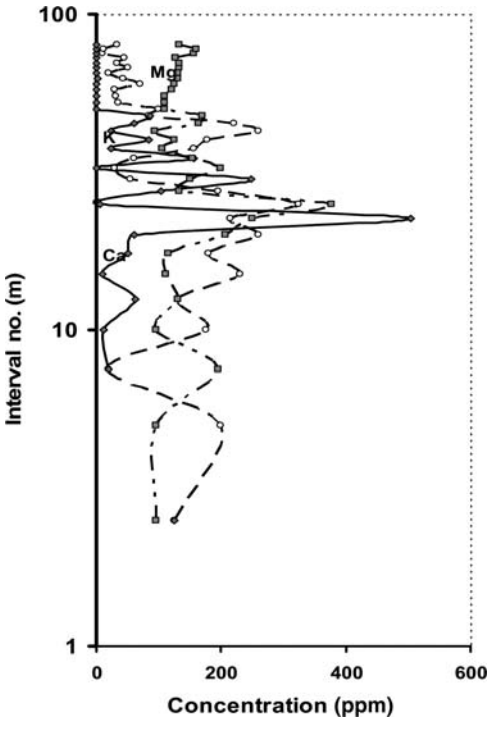

Fig. 13. Vertical Mg, K and Ca profiles of the Melheh salt pit (depth from top of the section).

euhedral carnallite and sylvite daughter minerals in their inclusions with their characteristic crystallographic appearance (Fig. 14). The primary polyphase inclusions, present in the sylvite crystals, represent brine evolution to the stage of potash saturation. Moreover, these observations along with the presence of mono-phase fluid inclusions in the primary minerals suggest an early stage of shallow burial diagenesis. Both the mono- and polyphase secondary inclusions are situated along the crystal boundaries of primary halite and have different compositions such as ferrous oxides, sulphates and diagenetic salt minerals.

Depositional model

Secular variations in the mineralogy of potash-bearing evaporite during Phanerozoic are discussed by many authors (e.g. Hardie 1990, 1991, 1996; Hryniv & Peryt 2003). Accordingly, in some periods $MgSO_4$ salts (such as polyhalite and kieserite) were the main potash minerals while $MgSO_4$-poor potash salts were dominant in other times (absence of $MgSO_4$ salts). The latter deposits, which contain halite, sylvite and carnallite as primary minerals and are usually entirely free from the primary Mg-sulphate salts, make up more than 60% of ancient potash deposits (Hardie 1990, 1991). However, as Hardie (1984) pointed out, these salts cannot be derived by normal evaporation of modern seawater or any similar sulphate-enriched brine. Hence, several hypotheses have been presented for the origin of these $MgSO_4$-poor salts, trying to explain these salts either as unusual marine evaporites or as altered marine evaporites. Among them, burial alteration of normal marine evaporites by groundwaters (Borchert 1977), bacterial sulphate reduction (e.g. Sonnenfeld 1984), seawater mixing with bicarbonate-rich river water (e.g. Valyashko 1972), and finally contemporaneous dolomitization of co-existing marine carbonates by seawater brines in a marine evaporite environment (Holland 1978), are most important. However, Hardie (1978) proposed a quite different explanation for this type of evaporite, particularly those deposited in rift and strike–slip basins. He suggested that upwelling $CaCl_2$ hydrothermal brines were the main source for $MgSO_4$-poor salts, as has been discovered in some modern analogous settings (e.g. Dead Sea trough, African rift basins). A similar concept has been put forward very recently by Hovland *et al.* (2006) with suggestive experimental data supporting this idea. The tectonic setting of Hardie's area had, presumably, the crucial conditions for evaporite deposition, such as arid climate and hydrologic closure of the depositional basin. In this system uplifted mountains encircled a series of elongated valleys, which were hydrologically closed sedimentary basins.

In this model, proposed by Hardie (1978), the basins were similar to the abundance of modern evaporite basins in central Iran, in which the uplifted mountains act as rainfall traps and barriers and the valley floors are local rain-shadow deserts. Deposition of thick evaporite deposits in these basins required rapid, active subsidence during the rapid evaporite accumulation and substantial inflow of brine (marine and/or non-marine) to the basin (Schreiber & Hsü 1980) with deposition and preservation that outpaces sand and mud influx into the basin (Hardie 1990). Seemingly, the evaporating basins were coastal depressions with their floors below sea level and with a constricted, very shallow inlet or a sort of permeable seal. As could be seen in some modern tectonically active closed basins, such as Dead Sea trough, Salton trough, Danakil Depression and Khur region in the southern border of the study area, deep circulating hot $CaCl_2$ brines are driven upward along faults and fracture zones by thermal anomalies along the axis of the extensional trough or by gravity from uplifted mountains that fed evaporite basins. The Khur region (Fig. 3), an old system of a closed continental rifting zone, which still shows some substantial

Table 2. *Br and SO_4^{2-} content in the halite layers (in bulk samples)*

Sample no.	Br(ppm)	SO_4%	Sample No.	Br(ppm)	SO_4%
1A	140	0.77	24	205	0.74
1	105	—	25	199	0.75
2	100	—	26	204	—
3	112	—	27	257	0.80
4	137	—	29	171	0.04
5	138	—	30	195	0.60
6	124	—	31	114	—
7	160	—	32	226	—
7a	100	—	34	216	0.21
8	158	—	35	203	—
11	198	—	36	86	0.61
12	179	—	37	208	—
13	176	3.14	38	184	—
13-1	156	—	39	197	2.06
13-2	162	—	40	—	215
14	143	0.89	41	—	204
15	186	—	42	222	6.10
16	232	2.94	43	211	—
17-1	163	—	44	219	—
17-2	205	—	45	224	—
18	195	—	46	50	0.67
19-1	182	—	47	242	1.19
20	168	—	48	208	—
21	197	—	49	197	—
22	190	—	64	168	—
23	220	3.08			

tectonic activity, is filled with about 7 km of Cenozoic marine evaporites, continental sediments and some volcanic extrusives.

In the study area, development of halite evaporites with substantial thickness (hundreds to thousands of metres), which suggests initial inflow of seawater along the narrow continental rift axis of the incipient ocean basin, initiated in Early Eocene time and continued up to the Middle Miocene in the isolated failed rift arms, oblique to the axis of divergence. Intermittent deposition of normal marine sediments (e.g. Qom Formation) on these continental sediments and marginal marine evaporites (LRF) demonstrates the full influx of the sea and the flooding of the subsiding margins of the divergent continents (Fig. 15). However, competition between marine and non-marine environments, at the edge of the encroaching sea, produced several cycles of abrupt and gradual transition from continental wadi sediments to marginal marine evaporite in the study area. This finally led to accumulation of marine evaporites of M1 of URF that, in turn, is gradually replaced by red beds of continental sediments of M2 and M3.

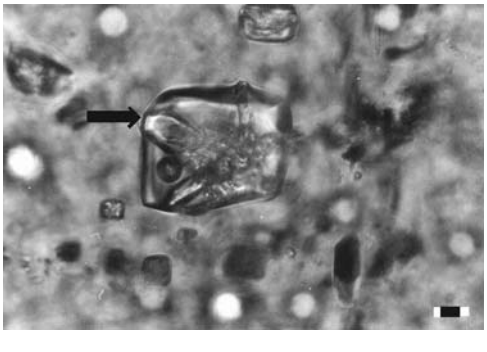

Fig. 14. Primary sylvite crystals that contain carnallite euhedral daughter mineral in its inclusions. Carnallite inclusion (arrow) shows its crystallographic characteristics (plane polarized light, scale bar 600 μm).

Brine origin and evolution

The brine origin and evolution in the modern and ancient continental rift basin has been addressed by several researchers, among them Hardie (1984, 1990) and Zak (1997). In particular the origin of $CaCl_2$ brine in the Dead Sea has been discussed by Zak (1997) and ascribed to mixing and chemical evolution of three basic brines. These include diagenetic brine formed by seawater evaporation, then modified by Mg + Ca exchange into Ca–Mg–Na–Cl–Br

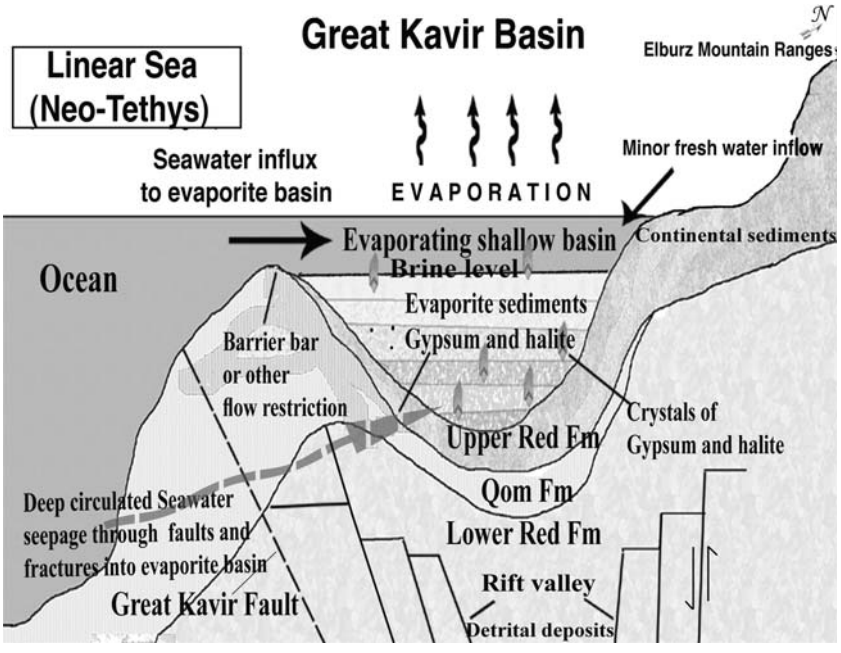

Fig. 15. Depositional model for evaporite deposition and associated marine and non-marine sediments in the Great Kavir Basin. Seawater, intermittently, recharged evaporite subbasins through land barriers and faults systems. In addition, modified seawater ($CaCl_2$ brines) was driven upward into the basin along faults and fracture zones by deep circulation. Arid climate and hydrologic closure enhanced evaporative concentration, and resulted in deposition of halite and $MgSO_4$-poor potash salts.

water. In this marine derived brine, Mg has been exchanged with the Ca from carbonate sediments and then most of the dissolved sulphate has been consumed by calcium sulphate precipitation. The other type of brine is altered meteoric water containing airborne sea salts. The third type is metamorphic brine that resulted from incongruent alteration and dissolution of hydrous evaporite minerals. The mixtures of these solutions experienced several progressive–regressive evaporation cycles with periodic precipitation of halite and sporadically of carnallite (Zak 1997).

In the Great Kavir Basin, which is an old continental rift setting, seawater moved into the subsurface through faults and fractures in the bedrock and after some alteration fluxed into isolated evaporite basins along hydraulic pathways. These marginal basins formed by extensive block faulting during rift opening and closure. These restricted basins, which temporarily were connected with the ocean and filled by normal seawater, were under the domination of the arid conditions and resulting evaporative concentration. On the other hand, in transit the deeper circulating seawater became heated and presumably reacted with the hot igneous and metamorphic bedrocks (Hardie 1990) and/or carbonate rocks (Zak 1997) before surfacing as $CaCl_2$ brine appropriate for precipitation of $MgSO_4$-poor salts. Thus, evaporating surface brines in the closed arid basins originated as mixtures of normal seawater plus the aforementioned hydrothermal $CaCl_2$ brine. As Hardie (1990) pointed out, 'only relatively small additions of $CaCl_2$ brines upwelling into the basin along faults and other permeable pathways are needed to convert a restricted body of seawater into $MgSO_4$-poor brine'. These $MgSO_4$-poor potash-bearing evaporites were deposited in marginal marine basins around the continental rift, which probably received an inflow of hydrothermal $CaCl_2$ brines. These basins were occasionally flooded with seawater, and seawater-derived hydrothermal brines leaked, more or less continually, through bedrock or another type of barrier by thermal or gravitational convection (Fig. 15). Some gypsum precipitated from such mixtures, and then, in the late stages of evaporation concentrated brines formed halite, sylvite and carnallite, that were precipitated with an absence of $MgSO_4$ salts. It seems that in the Great Kavir Basin, a long history of repeated tectonic movements and magmatism (from Early Cretaceous to Middle Miocene) was responsible for a very thick sequence of $MgSO_4$-poor potash evaporite deposits and its associated mixture of

both marine and continental sediments. Another indication of the contribution of hydrothermal waters to the brines forming $MgSO_4$-poor potash-bearing deposits in the study area is the higher than average concentration of Zn and Fe in the halite, as, for example the 943 ppm Fe, up to 1250 ppm Zn.

Conclusions

The Miocene evaporites studied in the Great Kavir Basin are $MgSO_4$-poor potash-bearing deposits, made up of cycles composed of halite, sylvite and carnallite with delicately and well-preserved primary depositional bottom growth textures. This conclusively demonstrates that primary, undersaturated inflow waters were $MgSO_4$-poor and also rules out any post depositional alteration mechanism as the cause of the lack of sulphate. However, the very soluble $CaCl_2$ mineral tachyhydrite ($CaCl_2 \cdot 2MgCl_2 \cdot 12H_2O$), which is typical of some of the $MgSO_4$-poor potash deposits, is absent in the study area. This could be ascribed to the moderate meteoric diagenesis that affected these deposits. These deposits are clearly primary precipitates and little altered since their accumulation. This conclusion is fully supported by textual evidence.

The primary potash of the study area formed syndepositionally, during or just after deposition by processes controlled by the existing depositional environment. According to field and petrographic examinations, the syndepositional origin of the potash salts in the Melheh salt pit is substantiated and the potash minerals formed primarily as bedded subaqueous deposits.

The stratigraphic relationships, petrographic textures, fluid inclusions and geochemistry of these potash-bearing evaporites demonstrate their primary origin. These observations lead us to conclude that the sylvite and carnallite are syndepositional in origin and formed as *in situ* subaqueous deposits, and the high Br content of those halite samples with well-preserved primary textures is an indication of a marine signature for parent brines. Moreover, Br values vary concordantly with the K and Mg that present preservation of a primary geochemical signature.

Seemingly, these evaporites were deposited in rift-related sub-basins formed by extensive block faulting during rift opening and closure. The latter were under the influence of upwelling $CaCl_2$ hydrothermal brine. These Zn- and Fe-rich hydrothermal brines were the main source for $MgSO_4$-poor salt deposition. Arid climate and hydrologic closure of this depositional basin enhanced evaporative concentration of the brines and salt deposition.

This paper is produced by a grant to the senior author from Tehran University, which is appreciated. B. C. Schreiber and A. Lomando provided invaluable comments and suggestions on the draft, for which we are sincerely grateful.

References

BELOV, A. A., GATINSKY, YU. G. & MOSSAKOVSKY, A. A. 1986. A précis on pre-Alpine tectonic history of Thetyan paleooceans. *Tectonophysics*, **127**, 197–211.

BODNAR, R. J. 1994. Philosophy of fluid inclusion analysis. *In*: DE VIVO, B. & FREZZOTTI, M. L. (eds) *Fluid Inclusions in Minerals, Methods and Applications*. Virginia Tech, Blacksburg, VA, 1– 6.

BORCHERT, T. H. 1977. On the formation of lower Cretaceous potassium salts and tachyhydrite in the Sergipe Basin (Brazil) with some remarks on similar occurrences in West Africa (Gabon, Angola, etc.). *In*: KELMM, D. D. & SCHNEIDER, H. J. (eds) *Time and Strata Bound Ore Deposits*. Springer, Berlin, 94–111.

BRAITSCH, O. 1971. *Salt Deposits: Their Origin and Composition*. Springer, Berlin.

BRAITSCH, O. & HERRMANN, A. G. 1963. Zür geochemie des broms in salinaren sedimenten. Teil II, die Bildungstem-peraturen primärer sylvin und carnallit-gestein. *Geochemica et Cosmochemica Acta*, **28**, 1081–1109.

BRULAND, K. W. 1983. Trace elements in sea-water. *In*: RILEY, J. P. & CHESTER, R. (eds) *Chemical Oceanography*. Academic Press, New York, 157–221.

CHESTER, R. 2000. *Marine Geochemistry.* Blackwell Science, Oxford.

DARI, M., BADAKHSHAN MOMTAZ, Q. & SAYAREH, A. 1993. *Potash exploration and equipping project in Iran for the Semnan and Garmsar Provinces*. Ministry of Mines and Industries, Report, **19**.

DARVISHZADEH, A. 1991. *Geology of Iran.* Neda University Press, Tehran.

DERCOURT, J., ZONENSHAIN, L. P. *ET AL*. 1986. Geological evolution of the Tethys belt from the Atlantic to the Pamirs since the Lias. *Tectonophysics*, **123**, B241–315.

DEWEY, J. F., HELMAN, M. L., TURCO, E., HUTTON, D. H. W. & KNOTT, S. D. 1989. Kinematics of The Western Mediterranean. *In*: COWARD, M. P., DIETRICH, D. & PARK, R. G. (eds) *Alpine Tectonics*. Geological Society Special Publication, **45**, 265–283.

GANSSER, A. 1974. The ophiolite mélange, a world-wide problem on Tethyan examples. Eclogae Geologiae Helvetiae, **67**, 429–507.

HARDIE, L. A. 1978. Evaporites, rifting and the role of $CaCl_2$ hydrothermal brines. *Geological Society of America*, Abstracts with Programs, **10**(7), 416.

HARDIE, L. A. 1984. Evaporites: marine or non-marine. *American Journal of Science*, **52**, 171–200.

HARDIE, L. A. 1990. The roles of rifting and hydrothermal $CaCl_2$ brines in the origin of potash evaporites: a hypothesis, *American Journal of Science*, **290**, 43–106.

HARDIE, L. A. 1991. On the significance of evaporites. *Annual Review of Earth and Planetary Sciences*, **19**, 131–168.

HARDIE, L. A. 1996. Secular variation in seawater chemistry: An explanation for the coupled variation in the mineralogies of marine limestones and potash evaporites over the past 600 my. *Geology*, **24**, 279–283.

HARDIE, L. A., LOWENSTEIN, T. K. & SPENCER, R. J. 1985. The problem of distinguishing between primary and secondary features in evaporites. *In*: SCHREIBER, B. C. & HARNER, L. (eds) *Sixth Symposium on Salt*. Salt Institute, Alexandria, VA, **1**, 11–39.

HOLLAND, H. D. 1978. *The Chemistry of the Atmosphere and Oceans*. Wiley-Interscience, New York.

HOLSER, W. T. 1979. Trace element and isotopes in evaporites. *In*: BURNS, R. G. (ed.) Marine Minerals. *Mineralogical Society of America, Reviews in Mineralogy*, **6**, 295–346.

HOVLAND, M., KUZNETSOVAW, T., RUESLA, H., KVAMME, B., JOHNSEN, H. K., FLADMARK, G. E. & HEBACH, A. 2006. Sub-surface precipitation of salts in supercritical seawater. *Basin Research*, **10**, 1365–2117.

HRYNIV, S. P. & PERYT, T. M. 2003. Sulfate cavity filling in the lower Werra anhydrite (Zechstein Permian), Zrada area, northern Poland: evidence for early diagenetic evaporate paleokarst formed under sedimentary cover. *Journal of Sedimentary Research*, **73**, 451–461.

JACKSON, M. P. A., CORNELIUS, R. R., CRAIG, C. H., GANSER, A., STOCKLIN, J. & TALBOT, C. J. 1990. *Salt Diapirs of the Great Kavir, central Iran*. Geological Society of America, Memoir, **177**.

KALHOR, R. 1961. Geology of Neogene formation in Varamin-Garmsar area and evaluation of Abardej Nose. *NIOC, Geological Report*, **233**.

KIRKLAND, D. W., DENISON, R. E. & DEAN, W. E. 2000. Parent brine of the Castile evaporites (Upper Permian), Texas and New Mexico. *Journal of Sedimentary Research*, **70**, 794–761.

KOVALEVICH, V. 1978. Fiziko-Khimicheskie uslovia formirovania soley Stebnikskogo kaliynogo mestorozhdenia: Kiev. *Naukova Dumka*.

KRINSLEY, D. B. 1970. *A Geomorphological and Palaeoclimatological study of the Playas of Iran*. Final reports for Air Force Cambridge Research Laboratories, part I, 329 and Part II.

KRINSLEY, D. B. 1974. Preliminary road alinement through the Great Kavir in Iran by repetitive ERTS-1 coverage [abstract]. *In*: *3rd Earth Resource Technology Satellite-1* Symposium, section A, Technical presentations. US National Aeronautical and Space Administration, Special Publications, **351**(1), 823.

KRINSLEY, D. B. 1976. Selection of a road alinement through the Great Kavir in Iran. *In*: *ERTS-1, a new Window on our Planet*. US Geological Survey, Professional Paper, **929**, 296–299.

KRINSLEY, D. B. 1977. *Use of ERTS-1 (Landsat-1) Images for Engineering Geologic Applications in North-central Iran*. US Geological Survey, Professional Paper, **1015**, 113–121.

LLEWELLYN, P. G. 1968. Dendritic halite pseudomorphs from the Keuper Marl of Leicestershire, England. *Sedimentology*, **11**, 293–297.

NATIONAL IRANIAN OIL COMPANY 1977. *Geological map of Iran, sheet 2 north-central Iran, with Explanatory text* (compiled by H. Huber). NIOC, Tehran, scale 1:100,000.

NEAL, J. T. 1969. Playa variation. *In*: MCGINNIS, W. G. & GORMAN, B. J. (eds) *Arid Lands in Perspective*. Arizona University Press, Tucson, **A2**, 14–44.

PERYT, M., PIERRE, C. & GRYNIV, S. P. 1998. Origin of polyhalite in the Zechstein (Upper Permian) Zrada platform (northern Poland). *Sedimentology*, **45**, 565–578.

PHILLIPS, F. G. 1956. *An Introduction to Crystallography*. Longmans, London.

RAHIMPOUR-BONAB, H. & ALIJANI, N. 2003. Petrography, diagenesis and depositional model for potash deposits of the north Central Iran, and use of bromine geochemistry as a prospecting tool. *Carbonates and Evaporites*, **18**, 19–28.

RAHIMPOUR-BONAB, H. & KALANTAR-ZADEH, Z. 2005. Origin of the secondary potash deposits; a case from Miocene evaporites of NW central Iran. *Journal of Asian Earth Sciences*, **25**, 157–166.

ROWLANDS, G. O., DELPAK, R. & GHAEM-MAGHAMI, E. 1984. The engineering properties of the saline soils of the Great Kavir in central Iran. *In*: BOYCE, J. R., MCKECHNIE, W. R. & SCHWARTZ, K. (eds) *Proceedings, 8th Regional Conference for Africa on Soil Mechanics and Foundation Engineering*, **8**, 337–341.

RUSSO, T. N. 1976. *Water Resources in the KAVIR National Park, Iran, 1975*. Iranian Department of Environment, Division of Nature Conservation.

SADEDIN, N. 1990. *Potash Exploration and Equipping Project in Iran for the Semnan Province*. Ministry of Mines and Industries, Reports.

SCHREIBER, B. C. & HSÜ, K. J. 1980. Evaporites. *In*: HOBSON, G. D. (ed.) *Developments in Petroleum Geology*, Applied Science, Barking, **2**, 87–138.

SCHREIBER, B. C. & EL TABAKH, M. 2000. Deposition and early alteration of evaporites. *Sedimentology*, **47**, Millennium Issue, 215–238.

SCOTESE, C. R. 1987. Phanerozoic reconstructions: a new look at the assembly of Asia. *Paleooceanographic Map Project Progress Report* 19–1286.

SHEARMAN, D. J. 1978. Evaporites of coastal sabkhas. *In*: DEAN, W. E. & SCHREIBER, B. C. (eds), *Marine Evaporites*. SEPM Short Course, **4**, 6–42.

SIEMANN, M. G., 1993. A practice-orientated way to produce diffraction reference cards using evaporate minerals. *Material Sciences Forum*, **136**, 27–32.

SIEMANN, M. G. & SCHRAMM, M. 2000. Thermodynamic modeling of the Br partition between aqueous solutions and halite. *Geochemica et Cosmochemica Acta*, **64**, 1681–1693.

SIEMANN, M. G. & ELLENDORFF, B. 2001. The composition of gases in fluid inclusions of Late Permian (Zechstein) marine evaporates in Northern Germany. *Chemical Geology*, **173**, 31–44.

SIEMANN, M. G. & SCHRAMM, M. 2002. Henry's and non-Henry's law behavior of Br in simple marine systems. *Geochemica et Cosmochemica Acta*, **66**, 1387–1399.

SOFFEL, H. C. & FORSTER, H. G. 1984. Polar wander of the Central-east Iran microplate including new results. *Neues Jahrbuch Geologische und Palaontologische Abhandlungen*, **168**, 165–172.

SONNENFELD, P. 1984. *Brines and Evaporites*. Academic Press, New York.

SONNENFELD, P. 1995. The color of rock salt – a review. *Sedimentary Geology*, **94**, 267–276.

SPENCER, R. J. 1987. Origin of $CaCl_2$ brines in Devonian formations, western Canada sedimentary basin. *Applied Geochemistry*, **2**, 373–384.

STOCKLIN, J. 1968. Salt deposits of the Middle East. *In*: MATTOX, R. B. (ed.) *Saline Deposits*. Geological Society of America, Special Paper, **88**, 158–181.

STOCKLIN, J. 1974. Possible ancient continental margins in Iran. *In*: BURK, C. A. & DRAKE, C. L. (eds) *The Geology of Continental Margins*. Springer, Berlin, 873–887.

VALYASHKO, M. G. 1972. Playa lakes – a necessary stage in the development of salt-bearing basin, *In*: RICHTER-BERNBURG, G. (ed.), *Geology of Saline Deposit*. UNESCO, Paris. Earth Sciences Series, **7**, 41–51.

VAUGHAN, H. B. 1893. A journey through Persia. *Royal Geographical Society Journal*, Supplementary Papers, **3**, 89–115.

WARREN, J. K. 1999. *Evaporites, their Evolution and Economics*, Blackwell Science, Oxford.

ZAK, I. 1997. Evolution of the Dead Sea brines. *In*: NIEMI, T. M., BEN-ABRAHAM, Z. & GAT, J. R. (eds) *The Dead Sea: The Lake and Its Setting*. Oxford University Press, Oxford, 133–144.